Journal of Nanoparticle Research (2006) 8: 729–736
DOI 10.1007/s11051-006-9097-2

Brief communication

Flame spray synthesis under a non-oxidizing atmosphere: Preparation of metallic bismuth nanoparticles and nanocrystalline bulk bismuth metal

Robert N. Grass and Wendelin J. Stark*
*Institute for Chemical and Bioengineering, ETH Zürich, Zurich, CH-8093, Switzerland; *Author for correspondence (Fax: +41-44-633-10-83; E-mail: wendelin.stark@chem.ethz.ch)*

Received 10 February 2006; accepted in revised form 22 March 2006

Key words: bismuth, metal nanoparticle, flame spray, reducing flame synthesis, nanocrystalline metal, combustion, nanoengineering

Abstract

Metallic bismuth nanoparticles of over 98% purity were prepared by a modified flame spray synthesis method in an inert atmosphere by oxygen-deficient combustion of a bismuth-carboxylate based precursor. The samples were characterized by X-ray diffraction, thermal analysis and scanning electron microscopy confirming the formation of pure, crystalline metallic bismuth nanoparticles. Compression of the as-prepared powder resulted in highly dense, nanocrystalline pills with strong electrical conductivity and bright metallic gloss.

Introduction

The current need for novel electronical and optical devices has triggered numerous research reports on the synthesis and use of metal and semiconductor nanoparticles (Kruis et al., 1998) for their improved properties, such as enhanced material strength (Suryanarayana, 1995; Sanders et al., 1997; Schiotz et al., 1999), altered magnetic or electronic behavior and quantum-confinement effects (Alivisatos, 1996; Madler et al., 2002c; Baribeau et al., 2005). Amongst others, the semimetal bismuth has been suggested for applications as thermoelectric material, optical and electro-optical devices (Wang et al., 2005) as well as in lubricant materials (Zhao et al., 2004), dry photo-tools (Wegner et al., 2002) and hall sensors (Sandhu et al. 2004). More specifically, decreasing the bismuth particle size results in a semimetal–semiconductor transition (Gallo et al., 1963; CostaKramer et al., 1997; Black et al., 2002). An enhanced thermoelectric effect may therefore be expected for decreased thermal conductivity while maintaining the electrical conductivity. Suitable materials were investigated by introducing nano-scale grain boundaries (Brochin et al., 1999; Dresselhaus et al., 1999; Heremans et al., 2000; Harman et al., 2002; Toprak et al., 2005).

A series of preparation methods has been developed to prepare the required bismuth nanoparticles. The synthesis of bismuth nanoparticles by vapor flow condensation (Wegner et al., 2002) resulted in products of high purity but was characterized by a limited production rate and product loss by wall deposition. Different liquid phase chemical reduction methods were applied at high yield for the synthesis of bismuth nanoparticles (Foos et al., 2000; Fang et al., 2000, 2001; Balan et al., 2004; Dellinger & Braun, 2004; Fu et al., 2005) but product contamination from remaining surfactants and solvent limited the accessible product purity. Similarly, bismuth nanoparticles

prepared by the dispersion of liquid bismuth in an inert solvent (Zhao et al., 2004) resulted in about 9 wt% organic residue.

Alternatively, high purity metal oxides (Rosner, 2005) are accessible by flame based processes at large production rates and relatively low costs. Silica and titania nanoparticles are currently produced commercially by flame aerosol synthesis and yield more than 2 million metric tons per year. The development of improved processes such as flame spray synthesis has enabled the preparation of a wide range of nanoparticulate products. Materials include complex oxides for use in optics, electronics and catalysis (Zachariah & Huzarewicz, 1991; Johannessen et al., 2004; Laine et al., 2005; Stark et al., 2005), metal salts and biomaterials (Grass & Stark, 2005; Huber et al., 2005; Loher et al., 2005) and noble metals (Keskinen et al., 2004; Makela et al., 2004).

In order to prepare non-oxidic materials such as carbon nanotubes (Vander Wal et al., 2000; Moisala et al., 2003) fuel rich or reducing flames were applied and resulted in the occurrence of metallic cobalt, iron and copper in the products. Similarly, mixtures of soot, carbon nanotubes and metallic nanoparticles were obtained from acetylene flames and an iron-carbonyl precursor (Height et al., 2004). These observations and recent reports on the gas phase reduction of copper (Nasibulin et al., 2001; Nasibulin et al., 2005), iron (Knipping et al., 2004) and nickel (Suh et al., 2005) indicate the possibility of manufacturing metallic nanoparticles in highly reducing flames.

We therefore investigated the preparation of metallic bismuth nanoparticles in a modified flame spray set-up while avoiding the undesired formation of soot. In order to control the atmosphere during production a flame spray reactor was operated in an oxygen-free glove-box filled with nitrogen. As-prepared bismuth powders were characterized by X-ray diffraction, scanning electron microscopy, thermal analysis and nitrogen adsorption. Compression of as-prepared bismuth nano powder to a bulk pill resulted in a nanocrystalline material of high relative density, bright metallic gloss and good electrical conductivity.

Experimental

Experimental set-up

A spray nozzle (adapted from Madler et al., 2002a) was placed in a glove-box (2 m^3) fed with nitrogen (PanGas, 99.999 %). The gas was recirculated by a vacuum pump (Busch, Seco SV1040CV) at about 20 m^3/h. CO_2 and H_2O were continuously removed from the recycle stream using two adsorption columns, packed with zeolite 4A and 13X (Zeochem), respectively. To avoid the accumulation of CO, NO and other impurities in the glove-box atmosphere a purge gas stream continuously passed through the box. A sinter metal tube (Haldenwanger, Halsic, inner diameter 25 mm) surrounding the flame allowed radial inflow of an inert mixing gas (N_2, 99.999 %) at a flow rate of 25 l/min and stable combustion (Figure 1, right). A mass spectrometer (Balzers, GAM 400) was applied for the detection of H_2, N_2, CO_2, NO, NO_2 and O_2. An oxygen concentration of below 100 ppm (volume/volume) was maintained during all experiments performed in the glove-box.

Bismuth (III) 2-ethylhexanoate (Stark et al., 2003; Grass et al., 2005) in mineral spirit (Strem, 28 wt% Bi) was diluted 2:1 (weight/weight) with tetrahydrofurane (Fluka, tech.) and filtered (Satorius, fluted filter type 288) prior to use. In a typical experiment, conversion of the bismuth-carboxylate based precursor into metallic bismuth nanoparticles was carried out by feeding the precursor at various feed rates (Table 1) by a micro annular gear pump (HNP Mikrosysteme, mzr-2900) into a premixed methane/oxygen flame (CH_4: 1.2 l/min, O_2: 2.2 l/min, PanGas tech.) after dispersion of the liquid by oxygen (Table 1; PanGas tech.). The product particles were separated from the off-gas using glass fiber filters (Schleicher & Schuell, GF6).

For reference, the bismuth-carboxylate based precursor was converted to bismuth (III) oxide by conventional flame spray pyrolysis (Madler & Pratsinis, 2002) using the set-up described above, but under ambient air instead of nitrogen and without the use of a surrounding and stabilizing sinter-metal tube (Figure 1, left).

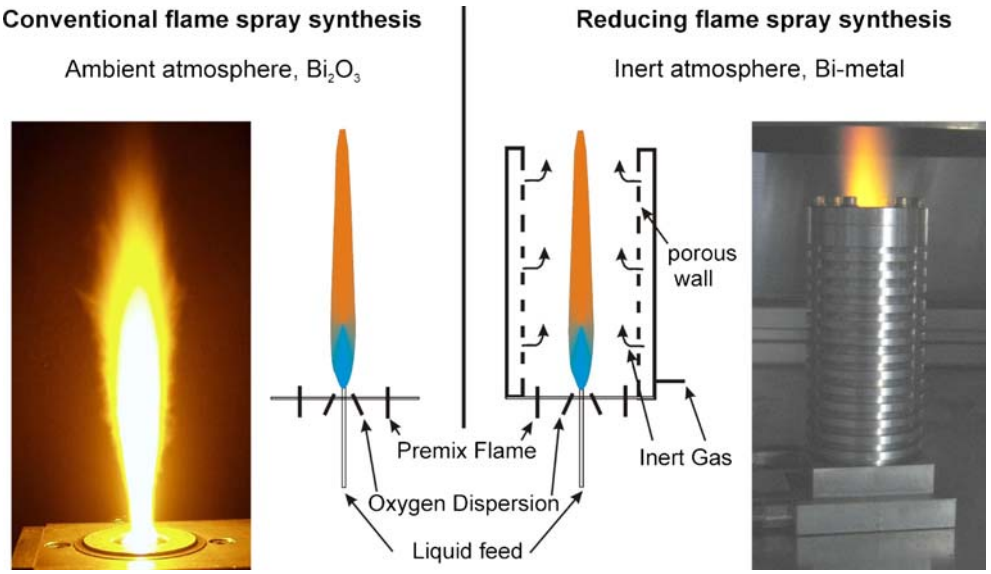

Figure 1. Flame spray synthesis under ambient conditions (left) and under a controlled nitrogen atmosphere (right).

Powder analysis

The nanoparticles were analyzed by X-ray diffraction (Stoe STADI-P2, Ge monochromator, $CuK_{\alpha\ 1}$, PSD detector), scanning electron microscopy (LEO 1530 Gemini, Accelerating voltage 10 kV), thermal gravimetric analysis (Linseis TG/STA-PT1600, 25–500 °C, 10 °C/min, air) and element microanalysis (LECO CHN-900). Nitrogen adsorption was performed on a Tristar (Micromeritics Instruments). The mean particle diameter d_{BET} (Table 1) was calculated from the specific surface area (SSA_{N2}) and the material bulk density (ρ) using the following correlation (Madler et al., 2002a):

$$d_{BET} = \frac{6}{SSA_{N2}\rho}$$

Scanning electron microscopy and thermal analysis were performed after passivation of the sample in air (Giesen et al., 2004). All other measurements were conducted in an inert atmosphere (< 100 ppm O_2).

Bulk bismuth samples were prepared by pressing as-prepared metallic powder (Table 1, Run 2, production rate 66 g/h) into a pill with a diameter of 12 mm using a uni-axial press at 370 or 74 MPa. The resistivity of the pill was measured using a 2-point method across the pill (Voltcraft, VC 220).

Table 1. Description of representative samples and process conditions

Run	Atmosphere	Conc. [wt % Bi]	Liquid [ml/min]	O_2[b] [l/min]	Prod. rate [g/h]	d_p[c] [nm]
1	Air	18.5	6	5	73	51
2	N_2[a]	18.5	6	5	66	127
3	N_2	3	6	5	10	52
4	N_2	18.5	4	4.2	44	102
5	N_2	18.5	3	3.3	33	102
6	N_2	18.5	2	2.5	22	111

[a]Oxygen concentration always below 100 ppm (volume/volume).
[b]All experiments were performed under a constant fuel to oxygen ratio $\phi = 2$ (Madler et al., 2002a).
[c]BET equivalent particle diameter calculated using Eq. (1). Error: ±10%.

Results

Combustion of bismuth-carboxylate precursor at a production rate of 75 g Bi_2O_3 per hour under ambient air conditions (Table 1, Run 1) resulted in the formation of a lightweight, bright yellow powder. Using the same reactor in a nitrogen atmosphere at equal feed rates (Table 1, Run 2) resulted in a gray-black powder that ignited spontaneously upon contact to air at room temperature. As previously observed (Madler & Pratsinis, 2002; Jossen et al., 2005) X-ray diffraction (Figure 2, bottom trace) confirmed that the yellow powder produced under ambient conditions consisted of nanocrystalline bismuth (III) oxide. The gray powder produced under inert conditions (Run 2) displayed X-ray reflections (Figure 2, middle trace) characteristic for metallic bismuth and no evidence of crystalline oxidic species or carbon modifications.

Scanning electron micrographs (Figure 3a, Run 2) showed nearly spherical nanoparticles of 20–80 nm diameter. The occurrence of some larger particles (Figure 3a, arrow) could be attributed to an inhomogeneous residence time distribution caused by mixing eddies (Madler et al., 2002b). The observed particle size is consistent with the

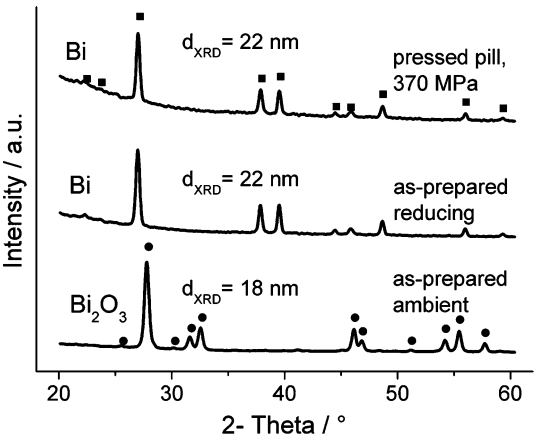

Figure 2. X-ray diffraction of as-prepared powders produced under ambient conditions (Bi_2O_3, bottom trace, Run 1), under an inert gas atmosphere (Bi, middle trace, Run 2) and of a pill pressed from bismuth nanopowder at 370 MPa (Bi, top trace). Reference data: Spheres: bismuth (III) oxide, squares: metallic bismuth.

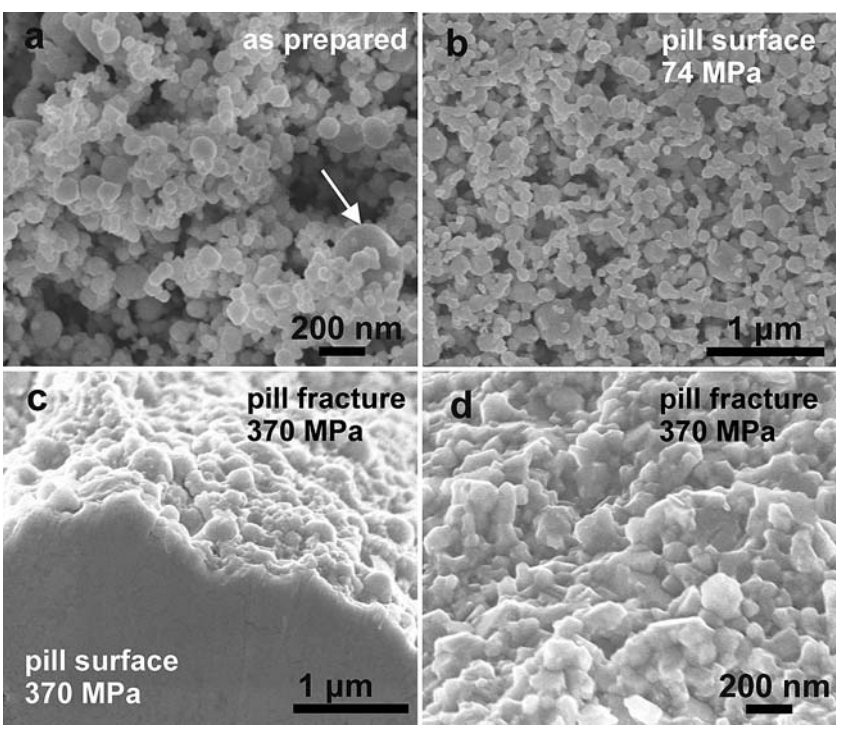

Figure 3. Scanning electron microscopy images of as-prepared bismuth powder (**a**) and pills pressed at 74 MPa (**b**) and at 370 MPa (**c**, **d**).

surface area equivalent diameter calculated according to Eq. (1). When changing the precursor flow rate at a constant fuel to oxygen ratio (Table 1, Runs 2, 4–6) the particle size remained nearly unchanged similar to previous observations for cerium oxide (Madler et al., 2002b). Dilution of the precursor (Table 1, Run 3) resulted in a significant decrease of the powder mean particle size (Mueller et al., 2003).

The metallic bismuth powder could be passivated by partial oxidation in ambient air (Giesen et al., 2004) and resulted in a mass gain of $\sim$1 wt% which was attributed to the formation of oxide layers protecting the powder from further oxidation. Thermal analysis (Figure 4) of the passivated sample further revealed that the protected material was stable in air up to about 170 °C where it ignited forming Bi_2O_3 with a total weight gain of 11.3 wt%.

Uniaxial compression of the bismuth powder at 74 MPa and room temperature resulted in a pill with a relative density of 73%. The morphology was observed by scanning electron microscopy images (Figure 3b) and confirmed an open structure consisting of particles of a similar size range to the as-prepared material. Increasing the pressure load to 370 MPa resulted in a strongly reflecting metallic pill (Figure 5). The pill was broken prior to investigation by scanning electron microscopy and revealed a very smooth pill surface (Figure 3c, lower half) and marginal porosity. This high degree of compression involving particle deformation

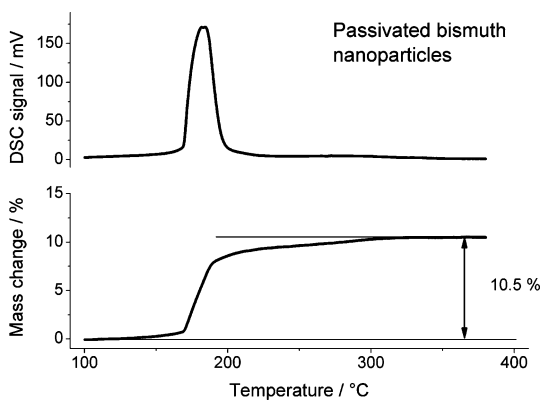

Figure 4. Thermal analysis of a representative, air-passivated bismuth sample (Run 2). Differential scanning calorimetry signal (top) and mass change due to oxygen uptake (bottom).

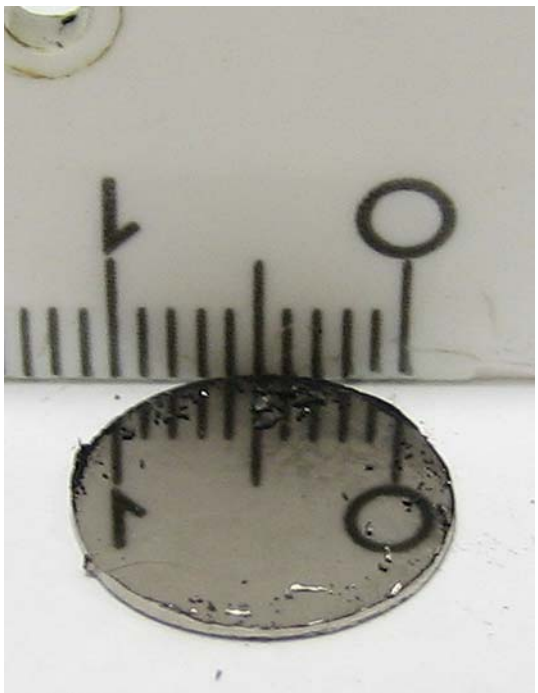

Figure 5. Bulk pill pressed from bismuth nanopowder pressed uniaxially at 370 MPa. The nanocrystalline metal is highly reflecting as can be seen from the mirror image of the white ruler (cm scale).

remained in agreement with a relative density of $>90\%$ as measured gravimetrically. Figure 3c (top) further shows the site of fracture revealing the nanocrystalline composition of the highly compacted bismuth metal pill. Figure 3d shows the fracture at higher magnification and displays strongly deformed grains. The grains are still of a similar size range as the as-prepared material. The observation is consistent with X-ray diffraction of the pressed pill (Figure 2, top trace) showing no peak narrowing (crystalline growth) upon densification. The electrical resistivity of the highly compacted pill was measured as $<0.01\ \Omega$ m.

Discussion

Preparation of metallic bismuth nanoparticles in flames

The formation of bismuth oxide nanoparticles from bismuth-2-ethylhexanoate in a flame under excess oxygen (Jossen et al., 2005; Madler &

Pratsinis, 2002) can be described by the following reaction equation:

$$2Bi(C_8H_{15}O_2)_3 + 66O_2 \rightarrow Bi_2O_3 + 48CO_2 + 45H_2O \quad (2)$$

Using a nitrogen atmosphere, the amount of oxygen accessible for combustion can be limited to the oxygen initially fed to the flame. Therefore, the different constituents (CO, H_2, Bi) are now competing for oxygen. The Gibbs energy of reaction $\Delta_r G$ (Table 2) may be calculated both at the maximum flame temperature (~1500 °C) and the filter temperature (~70 °C). Comparison of the corresponding oxidation reactions (Table 2) involving one oxygen each shows that under limited oxygen availability the thermodynamically preferred reaction product is metallic bismuth.

More specifically, the different $\Delta_r G$ values (Table 2, Sandler, 1999) show that combustion of hydrogen or CO is preferred to the oxidation of bismuth. This preference is even amplified at higher temperatures (e.g. 1500 °C). It may be attributed to the positive molar heat capacity of reaction ($\Delta_r C_p$) and stronger negative reaction entropy ($\Delta_r S^0$) of the oxidation of bismuth if compared to the oxidation of hydrogen or CO (Table 2).

Under the oxygen limited conditions applied here, the bismuth-carboxylate is therefore converted into a mixture of CO, CO_2, H_2, H_2O and metallic bismuth nanoparticles. The presence of reducing gases has been further confirmed by mass spectroscopy.

Product characterization

The purity of the as-prepared bismuth nanoparticles could be calculated from the weight gain due to oxidation. Assuming full oxidation of metallic bismuth to bismuth (III) oxide results in a theoretical weight gain of 11.5 wt%. For the observed mass gain of 11.3 wt% a sample purity of >98% metallic bismuth could be calculated. Using the density of Bi_2O_3 the thickness of the corresponding passivating oxide layer was estimated as ~3–4 layers of Bi_2O_3 equivalent to a weight gain of 1 wt%. The high purity corroborated the absence of solid or adsorbed carbonaceous species and illustrated the feasibility of producing carbon free metallic nanoparticles in flames. This observation was further confirmed by element analysis showing negligible amounts of carbon (0.1 wt%) in the as-prepared product. The present results indicate that the high temperatures in flames suppressed kinetic effects and metallic bismuth nanoparticles were formed according to equilibrium thermodynamics.

The independence of particle size on production rate under constant fuel to oxygen ratio and precursor concentration (Runs 2, 4–6) was consistent with prior work on ceria nanoparticles (Madler et al., 2002b) and confirmed the similarity of the metal nanoparticle formation in flames to the preparation of oxidic nanoparticles. The primary particle size could be changed by the precursor concentration as described previously in detail for metal oxide nanoparticles (Mueller et al., 2003). It has been shown both theoretically (Tsantilis et al., 2002) and experimentally (Arabi-Katbi et al., 2001) that oxidic nanoparticles are formed by aggregation and sintering. The results presented here indicate that the synthesis of metallic bismuth nanoparticles follow the same evolution. Due to the very low melting point of metallic bismuth (271 °C) sintering even occurred in late stages of the flame and relatively large primary particles were formed (Table 1, Figure 3a). The small crystallite size of the particles (22 nm for Run 2) in comparison to the primary particle size

Table 2. Thermodynamic data (Lide, 1997)

Reaction	$\Delta_r G$ (70 °C)[a] [kJ/mol]	$\Delta_r G$ (1500 °C)[a] [kJ/mol]	$\Delta_r C_p$ [J/mol/K]	$\Delta_r S^0$ [J/mol/K]
$2\ H_2 + O_2 = 2\ H_2O$	−454	−355	−19.8	−89
$2\ CO + O_2 = 2\ CO_2$	−507	−279	−13.4	−173
$4/3\ Bi + O_2 = 2/3\ Bi_2O_3$	−320	−46	12.3	−180
$2/3\ Bi_2O_3 + 2\ CO = 4/3\ Bi + 2\ CO_2$	−187	−233	−26	6.8
$2/3\ Bi_2O_3 + 2\ H_2 = 4/3\ Bi + 2\ H_2O$	−133	−309	−32	90.8

[a]Calculated applying the 2nd Ulich approximation (Sandler, 1999).

(127 nm from BET) indicated the formation of polycrystalline particles consisting of numerous single crystals.

The formation of a highly dense bulk pill from the as-prepared bismuth metal powder may be explained in terms of facile deformation of the grains in order to achieve optimal packing. The extensive grain deformation even at room temperature could be accredited to the low melting point of this very soft metal (T_M = 271 °C; Moos hardness = 2). These results show that metallic bismuth nanoparticles can be used for the fast and simple preparation of bulk nanocrystalline metals without the need of sintering, which would lead to significant grain and crystallite growth (Chen & Wang, 2000).

Conclusions

Flame combustion of a bismuth-carboxylate precursor in an inert atmosphere under limited oxygen supply resulted in reducing combustion conditions and the formation of pure metallic bismuth nanoparticles with mean particle sizes between 50 and 120 nm. The nanoparticles could be pressed to highly dense pills exhibiting metallic gloss and showing electrical conductivity. These properties may suggest applications of flame made metallic bismuth nanoparticles for soldering alloys and as a suitable candidate for thermoelectric applications.

Acknowledgements

This work was financed by the ETH Zürich. The authors would like to thank Urs Krebs and Hans-Peter Schläpfer for reactor construction and Prof. L.J. Gaukler for SEM measuring time.

References

Alivisatos A.P., 1996. Science 271, 933–937.
Arabi-Katbi O.I., S.E. Pratsinis, P.W. Morrison & C.M. Megaridis, 2001. Comb. Flame 124, 560.
Balan L., R. Schneider, D. Billaud, Y. Fort & J. Ghanbaja, 2004. Nanotechnology 15, 940.
Baribeau J.M., N.L. Rowell & D.J. Lockwood, 2005. J. Mater. Res. 20, 3278.
Black, M.R., Y.M. Lin, S.B. Cronin, O. Rabin & M.S. Dresselhaus, 2002. Phys. Rev. B 65.
Brochin F., X. Devaux, J. Ghanbaja & H. Scherrer, 1999. Nanostruct. Mater. 11, 1.
Chen I.W. & X.H. Wang, 2000. Nature 404, 168.
Costa-Krämer J.L., N. García & H. Olin, 1997. Phys. Rev. B 55, 12910.
Dellinger T.M. & P.V. Braun, 2004. Chem. Mat. 16, 2201.
Dresselhaus M.S., G. Dresselhaus, X. Sun, Z. Zhang, S.B. Cronin & T. Koga, 1999. Phys. Solid State 41, 679.
Fang J.Y., K.L. Stokes, J. Wiemann & W.L. Zhou, 2000. Mater. Lett. 42, 113.
Fang, J.Y., K.L. Stokes, W.L.L. Zhou, W.D. Wang & J. Lin, 2001. Chem. Commun. 1872.
Foos E.E., R.M. Stroud, A.D. Berry, A.W. Snow & J.P. Armistead, 2000. J. Am. Chem. Soc. 122, 7114.
Fu R.L., S. Xu, Y.N. Lu & J.J. Zhu, 2005. Cryst. Growth Des. 5, 1379.
Gallo C.F., B.S. Chandrasekhar & P.H. Sutter, 1963. J. Appl. Phys. 34, 144.
Giesen B., H.R. Orthner, A. Kowalik & P. Roth, 2004. Chem. Eng. Sci. 59, 2201.
Grass, R.N., E.K. Athanassiou & W.J. Stark, 2005. EP Patent application 05 019287.1.
Grass, R.N. & W.J. Stark, 2005. Chem. Commun. 1767.
Harman T.C., P.J. Taylor, M.P. Walsh & B.E. LaForge, 2002. Science 297, 2229.
Height M.J., J.B. Howard, J.W. Tester & J.B.V. Sande, 2004. Carbon 42, 2295.
Heremans J., C.M. Thrush, Y.M. Lin, S. Cronin, Z. Zhang, M.S. Dresselhaus & J.F. Mansfield, 2000. Phys. Rev. B 61, 2921.
Huber, M., W.J. Stark, S. Loher, M. Maciejewski, F. Krumeich & A. Baiker, 2005. Chem. Commun. 648.
Johannessen T., J.R. Jenson, M. Mosleh, J. Johansen, U. Quaade & H. Livbjerg, 2004. Chem. Eng. Res. Des. 82, 1444.
Jossen R., S.E. Pratsinis, W.J. Stark & L. Madler, 2005. J. Am. Ceram. Soc. 88, 1388.
Keskinen H., J.M. Makela, M. Vippola, M. Nurminen, J. Liimatainen, T. Lepisto & J. Keskinen, 2004. J. Mater. Res. 19, 1544.
Knipping J., H. Wiggers, B.F. Kock, T. Hulser, B. Rellinghaus & P. Roth, 2004. Nanotechnology 15, 1665.
Kruis F.E., H. Fissan & A. Peled, 1998. J. Aerosol. Sci. 29, 511 .
Laine R.M., J. Marchal, H.P. Sun & X.Q. Pan, 2005. Adv. Mater. 17, 830.
Lide D.R., 1997. CRC Handbook of Chemistry and Physics, 78th edn. CRC Press.
Loher S., W.J. Stark, M. Maciejewski, A. Baiker, S.E. Pratsinis, D. Reichhardt, F. Maspero, F. Krumeich & D. Günther, 2005. Chem. Mater. 17, 36.
Madler L., H.K. Kammler, R. Mueller & S.E. Pratsinis, 2002a. J. Aerosol. Sci. 33, 369.
Madler L. & S.E. Pratsinis, 2002. J. Am. Ceram. Soc. 85, 1713 .
Madler L., W.J. Stark & S.E. Pratsinis, 2002b. J. Mater. Res. 17, 1356.

Madler L., W.J. Stark & S.E. Pratsinis, 2002c. J. Appl. Phys. 92, 6537.
Makela J.M., H. Keskinen, T. Forsblom & J. Keskinen, 2004. J. Mater. Sci. 39, 2783.
Moisala A., A.G. Nasibulin & E.I. Kauppinen, 2003. J. Phys.-Condes. Matter. 15, S3011.
Mueller R., L. Madler & S.E. Pratsinis, 2003. Chem. Eng. Sci. 58, 1969.
Nasibulin A.G., P.P. Ahonen, O. Richard, E.I. Kauppinen & I.S. Altman, 2001. J. Nanopart. Res. 3, 385.
Nasibulin A.G., L.I. Shurygina & E.I. Kauppinen, 2005. Colloid J. 67, 1.
Rosner D.E., 2005. Ind. Eng. Chem. Res. 44, 6045.
Sanders P.G., C.J. Youngdahl & J.R. Weertman, 1997. Mater. Sci. Eng. A-Struct. Mater. Prop. Microstruct. Process. 234, 77.
Sandler S.I., 1999. Chemical and Engineering Thermodynamics. New York: John Wiley & Sons.
Sandhu A., K. Kurosawa, M. Dede & A. Oral, 2004. Jpn. J. Appl. Phys. Part 1(43), 777.
Schiotz J., T. Vegge, F.D. Di Tolla & K.W. Jacobsen, 1999. Phys. Rev. B 60, 11971.
Stark W.J., J.D. Grunwaldt, M. Maciejewski, S.E. Pratsinis & A. Baiker, 2005. Chem. Mat. 17, 3352.
Stark W.J., L. Madler, M. Maciejewski, S.E. Pratsinis & A. Baiker 2003. Chem. Commun. 588–589.
Suh Y.J., H.D. Jang, H.K. Chang, D.W. Hwang & H.C. Kim, 2005. Mater. Res. Bull. 40, 2100.
Suryanarayana C., 1995. Int. Mater. Rev. 40, 41.
Toprak M.S., Y. Zhang, Y. Jo, D.K. Kim & M. Muhammed, 2005. Solid State Phenom. 101–102, 197.
Tsantilis S., H.K. Kammler & S.E. Pratsinis, 2002. Chem. Eng. Sci. 57, 2139–2156.
Vander Wal R.L., T.M. Ticich & V.E. Curtis, 2000. Chem. Phys. Lett. 323, 217.
Wang Y.W., B.H. Hong & K.S. Kim, 2005. J. Phys. Chem. B 109, 7067.
Wegner K., B. Walker, S. Tsantilis & S.E. Pratsinis, 2002. Chem. Eng. Sci. 57, 1753.
Zachariah M.R. & S. Huzarewicz, 1991. Combust. Flame 87, 100.
Zhao Y.B., Z.J. Zhang & H.X. Dang, 2004. Mater. Lett. 58, 790.